Production and propagation of secondary antideuteron in the Galaxy

Luis Fernando Galicia Cruztitla† **and Diego Mauricio Gómez Coral**⋆

Instituto de Física, Universidad Nacional Autónoma de México, Circuito de la Investigación Científica, Ciudad Universitaria, CDMX, 04510, Mexico

† luisfergac@ciencias.unam.mx , ⋆ dgomezco@fisica.unam.mx

22nd International Symposium on Very High Energy Cosmic Ray Interactions (ISVHECRI 2024)
Puerto Vallarta, Mexico, 8-12 July 2024
doi:10.21468/SciPostPhysProc.?

Abstract

This work reviews the current state of the antideuteron ($\bar{d}$) production cross-sections in cosmic ray interactions and its uncertainties, considering the coalescence model and measurements in accelerator experiments. These cross-sections have been included in a simulation of cosmic rays propagation in the Galaxy using `GALPROP v.57`, with updated parameters of the diffusive reacceleration model. An estimation of the expected antideuteron flux at Earth is presented.

Received Date
Accepted Date
Published Date

Contents

1 Introduction

Cosmic Rays (**CRs**) produced in stars and accelerated into the Interstellar Medium (**ISM**) in supernova remnants (**SNRs**) are called *primary cosmic rays*. Composed mostly of protons (p) and Helium (He), these primary particles interact with the **ISM** through inelastic collisions producing *secondary cosmic rays* [1]. In a Universe dominated by matter, and within the Standard Model of particles (**SM**), the production of antimatter could only be possible through the nuclear interactions of **CRs** with the **ISM**, i.e. antimatter is expected to be of *secondary* origin. However, Dark Matter (**DM**) models predict $\bar{d}$ production by annihilation or decay of **DM** particles in the Galaxy [2]. This additional primary $\bar{d}$ production would be observed as an excess to the secondary component at energies below 1 GeV [3]. Interestingly, the Alpha Magnetic Spectrometer (AMS-02) detector onboard the International Space Station (**ISS**) has reported 7 $\bar{d}$ candidates in the energy region above 1 GeV [4]. Although a **DM** origin of these $\bar{d}$ seems to be in tension with the observations, a clear interpretation of the results requires a good estimation of the secondary component. Therefore, in this work a review of the $\bar{d}$ production cross sections within the coalescence model, and an estimation of the flux after propagation in the Galaxy are presented.

2 Transport of galactic CRs

Charged **CRs** particles propagate in the Galaxy following a diffusive process due to perturbations in the magnitude and direction of the magnetic fields of the different regions of the Galaxy. As a consequence, **CRs** confined time in the galactic volume is on the order of megayears [5]. The dynamics of the propagation of **CRs** in the Galaxy is modeled by the *transport equation* [6]:

$$\frac{\partial \psi(\bar{r},p,t)}{\partial t} = Q(\bar{r},p) + \nabla \cdot [D_{xx}\nabla\psi - \bar{V}\psi] + \frac{\partial}{\partial p}\left[p^2 D_{pp}\frac{\partial}{\partial p}\frac{\psi}{p^2}\right] - \frac{\partial}{\partial p}\left[\frac{dp}{dt}\psi - \frac{1}{3}p\nabla\cdot\bar{V}\psi\right] - \frac{\psi}{\tau_f} - \frac{\psi}{\tau_d}. \tag{1}$$

On the left side, we have the time variation of the ψ function that represents the density of particles per unit of momentum. On the right side, the first term ($Q(\bar{r},p)$) represents the sources of **CRs** such as **SNRs** or secondary production by nuclear interactions. The second term corresponds to the diffusion and convective part, where D_{xx} is the diffusion coefficient and V is the convection velocity. The third term refers to the diffusive reacceleration process, with a diffusion coefficient in the momentum space D_{pp}. The fourth term describes energy loss processes, in particular, momentum loss due to interactions with the **ISM** and losses due to non-uniform convection. Finally, the last two terms indicate losses by fragmentation or annihilation and losses by radioactive decay respectively.

To simulate the propagation process of $\bar{d}$ in the Galaxy, the open source code `GALPROP v.57` [7] is used. `GALPROP` solves the transport equation numerically, and introduces current astrophysical models and data to make the simulation more realistic. For the present study, a two-dimensional diffusion halo with cylindrical symmetry is considered. The parameters on the transport equation (including the size of the Galaxy, and diffusion coefficient, among others), were set according to Boschini *et al.* [8].

3 Secondary antideuteron production

3.1 Coalescence model

The coalescence model postulates that an $\bar{d}$ can be formed if an antiproton ($\bar{p}$) and an antineutron ($\bar{n}$) produced after an interaction are close in phase space within a volume determined by a radius in momentum p_0 [9, 10], known as the coalescence momentum. In this way, a primary accelerated p or He, with enough energy, interacting with a p or He of the **ISM**, might produce a sequence of $\bar{p}$ and $\bar{n}$ that could coalesce to form $\bar{d}$ or increasingly heavier antinuclei.

As a first analytical approach, the distribution of the $\bar{p}$-$\bar{n}$ pair momentum can be seen as the product of two independent isotropic distributions, without correlation [11]. In this way, the $\bar{d}$ spectrum is given by

$$\gamma_{\bar{d}} \frac{\partial^3 N_{\bar{d}}}{dp^3_{\bar{d}}} = \frac{4\pi}{3} p_0^3 \left(\gamma_{\bar{p}} \frac{\partial^3 N_{\bar{p}}}{dp^3_{\bar{p}}} \right) \left(\gamma_{\bar{n}} \frac{\partial^3 N_{\bar{n}}}{dp^3_{\bar{n}}} \right), \tag{2}$$

where $\frac{\partial^3 N}{dp^3}$ represents the differential yield per event of particle ($\bar{p}$, $\bar{n}$ and $\bar{d}$) in terms of momentum, γ is the Lorentz factor for each particle and p_0 is the coalescence momentum. However, the production of antinuclei pairs in nuclear collisions is not independent or isotropic, i.e. they are correlated [12]. To take these correlations into account, the coalescence mechanism to form $\bar{d}$ is simulated on an event-by-event basis, using $\bar{p}$-$\bar{n}$ pairs produced in p-p, p-He, He-p, and He-He collisions with Monte Carlo (**MC**) generators. Collisions simulated with **MC** generators follow interaction models that already contain correlations between products [13]. To generate a new $\bar{d}$ from any $\bar{p}$-$\bar{n}$ pair, the center of mass momentum of the pair p_{cm} should be less than the coalescence momentum, i.e. $p_{cm} < p_0$. The value of p_0 is chosen in a way the final $\bar{d}$ differential cross section is in agreement to accelerator measurements [12]. On the other hand, the condition on the $\bar{p}$-$\bar{n}$ pair separation boundary (Δx) is enforced by allowing only $\bar{d}$ that are generated within a radius of ~ 2 fm to coalesce. Here, **CRs** collisions and $\bar{d}$ production simulated with `EPOS-LHC` generator and a coalescence afterburner by Shukla *et al.* [14] and Gomez-Coral *et al.* [12] were used.

3.2 Secondary source term

The secondary source term Q (see Eq. 1) for $\bar{d}$ production by **CRs** collisions can be written as follows:

$$Q^{sec}_{\bar{d}}(E^{\bar{d}}_{kin}, \mathbf{r}) = \sum_{i\in\{p,He,\bar{p}\}} \sum_{j\in\{p,He\}} 4\pi n_j(\mathbf{r}) \int_{E^{(i,j)}_{kin(\bar{d})}}^{\infty} \frac{d\sigma_{i,j}(E_{kin(i)}, E^{\bar{d}}_{kin})}{dE^{\bar{d}}_{kin}} \Phi_i(E_{kin(i)}, \mathbf{r})\, dE_{kin}, \tag{3}$$

where n_j is the particle density of the **ISM**, $E_{kin(i)}$ denote the kinetic energy per nucleon of the incident particles, Φ_i the incident flux of **CRs** (p and He) and $\left(\frac{d\sigma_{prod}}{dE^{\bar{d}}_{kin}}\right)_{i,j}$ corresponds to the differential cross section for $\bar{d}$ with $E^{\bar{d}}_{kin}$ the kinetic energy per nucleon for $\bar{d}$ [15]. The secondary source term convolves the $\bar{d}$ differential production cross section obtained using `EPOS-LHC` and the coalescence model [16] (see Sec. 3.1).

4 Results

4.1 Differential cross section production and source term for $\bar{d}$

From the limited discrete data generated with EPOS-LHC and the coalescence simulation of $\bar{d}$ published by Shukla *et al* [14] (color points in Fig.1 (a)), a polynomial fit was performed over a continuous interval of $\bar{d}$ kinetic energy per nucleon, for every set of data points per projectile kinetic energy (color lines in Fig.1 (a)). Then, the parameters obtained from this fit were interpolated as a function of the projectile kinetic energy per nucleon, to get a complete parametrization of the $\bar{d}$ production cross sections.

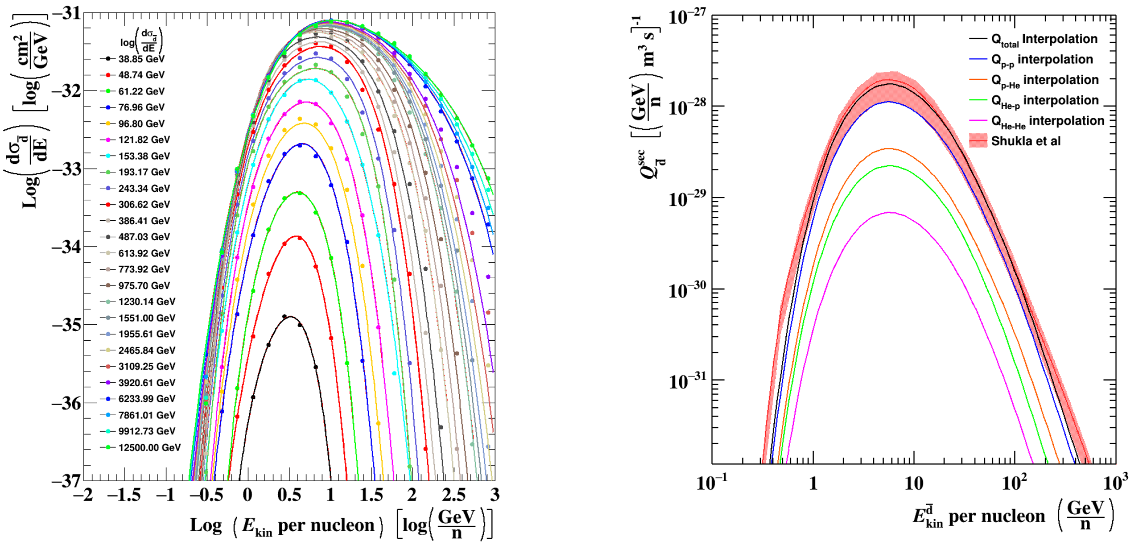

(a) (b)

Figure 1: (a): $\bar{d}$ production differential cross section ($\frac{d\sigma_{\bar{d}}}{dE}$), as a function of $\bar{d}$ kinetic energy per nucleon in log-log scale, for different projectile energies. (b): Total secondary $\bar{d}$ source term (black line) and contributions from all types of **CRs** collisions (color lines) calculated with a parametrization function and compared to [14] (red band).

Then, the secondary source term was estimated using the $\bar{d}$ production cross section parametrization in Eq. 3, and was compared to [14]. The results are shown in Fig. 1 (b), where can be seen that both results (solid black line and red solid line) are in agreement for most of the $\bar{d}$ energy range.

4.2 Expected $\bar{d}$ flux

Finally, the $\bar{d}$ production cross section parametrization was implemented in GALPROP v.57 (Sec. 2) where $\bar{d}$ were propagated using updated propagation parameters. Solar modulation was modeled using the Force Field approximation [17]. ϕ_F was obtained from a fit of the model to AMS-02 $\bar{p}$ measurements [18]. The resulting Top-Of-Atmosphere TOA fluxes as a function of kinetic energy per nucleon for $\bar{p}$ (blue solid line) and $\bar{d}$ (red line) are shown in Fig. 2 along with AMS-02 $\bar{p}$ data [18] (black points) and AMS-02 $\bar{d}$ sensitivity [19] (green lines), considering the projection with a superconducting-magnet configuration. The red band in Fig. 2 represents the $\bar{d}$ cross section uncertainty estimated in [14] as 35% above and 45% below the expected flux.

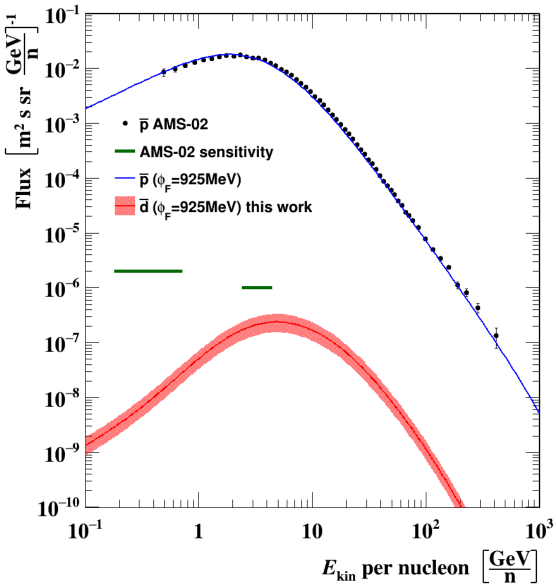

Figure 2: Estimated secondary $\bar{d}$ flux with GALPROP v.57 (red line) and its uncertainties associated with cross sections (red band). For comparison, the $\bar{d}$ AMS-02 sensitivity is shown as green lines [19]. The modulated $\bar{p}$ flux calculated with GALPROP v.57 (blue line) is compared to $\bar{p}$ AMS-02 data [18] (black points).

5 Conclusions

The expected secondary $\bar{d}$ flux was estimated by performing a parametrization of the $\bar{d}$ production cross sections as a function of $\bar{d}$ kinetic energy and projectile energy, using **MC** data generated by [14]. To propagate $\bar{d}$ in the Galaxy, GALPROP v.57 was used along with the latest propagation parameters from [8]. The final results are presented in Fig. 2, where it can be seen the AMS-02 sensitivity reported in [19] is above the calculated $\bar{d}$ flux by a factor of 3. A similar result is obtained when an AMS-02 sensitivity, with a permanent-magnet configuration for 11 years, is considered [20]. Previous calculations are consistent with this result [21,22]. This suggests the $\bar{d}$ candidates reported by AMS-02 [4] would not come from a secondary origin. However, measurements in $\bar{d}$ production cross sections for projectile energies between 100 to 200 GeV are necessary to corroborate a coalescence momentum dependence with projectile energy [12]. A significantly higher $\bar{d}$ flux can be obtained by considering a constant p_0 [23]. Interestingly, a recent AMS-02 sensitivity projection for 2030 with a planned detector upgrade is close to the maximum of our secondary $\bar{d}$ flux estimation [20] (Fig. 2), suggesting that AMS-02 would be practically background-free for possible antideuteron observation coming from dark matter or new astrophysical production mechanisms.

Acknowledgements

The authors thank Anirvan Shukla for sharing the **MC**-generated data. This work was supported by UNAM-PAPIIT IA101624 and by CONAHCYT under grant CBF2023-2024-118. LFGC thanks the support from CONAHCYT-[CVU-937792] scholarship and PAEP-UNAM.

References

[1] C. Grupen, *Astroparticle Physics*, Springer International Publishing, ISBN 9783030273392, doi:10.1007/978-3-030-27339-2 (2020).

[2] F. Donato *et al.*, *Antideuteron fluxes from dark matter annihilation in diffusion models*, Phys. Rev. D **78**(4) (2008), doi:10.1103/PhysRevD.78.043506.

[3] P. v. Doetinchem *et al.*, *Cosmic-ray antinuclei as messengers of new physics: status and outlook for the new decade*, J. Cosmol. Astropart. Phys. **2020**(08), 035 (2020), doi:10.1088/1475-7516/2020/08/035.

[4] S. Ting, *Latest results from ams experiment on the ISS*, CERN Colloquium presentation, https://indico.cern.ch/event/1275785/ (2023).

[5] P. Blasi, *Charged particles in magnetic fields and cosmic ray transport* (2023), doi:10.48550/arXiv.2307.11640.

[6] L. Šerkšnytė *et al.*, *Reevaluation of the cosmic antideuteron flux from cosmic-ray interactions and from exotic sources*, Phys. Rev. D **105**(8) (2022), doi:10.1103/PhysRevD.105.083021.

[7] T. A. Porter *et al.*, *The GALPROP cosmic-ray propagation and nonthermal emissions framework: Release v57*, ApJS **262**(1), 30 (2022), doi:10.3847/1538-4365/ac80f6.

[8] M. J. Boschini *et al.*, *Inference of the local interstellar spectra of cosmic-ray nuclei $Z \leq 28$ with the GalProp–HelMod framework*, ApJS **250**(2), 27 (2020), doi:10.3847/1538-4365/aba901.

[9] S. T. Butler and C. A. Pearson, *Deuterons from high-energy proton bombardment of matter*, Phys. Rev. **129**(2), 836 (1963), doi:10.1103/PhysRev.129.836.

[10] L. Csernai and J. I. Kapusta, *Entropy and cluster production in nuclear collisions*, Phys. Rep. **131**(4), 223 (1986), doi:10.1016/0370-1573(86)90031-1.

[11] P. Chardonnet *et al.*, *The production of anti-matter in our galaxy*, Phys. Lett. B **409**(1–4), 313 (1997), doi:10.1016/S0370-2693(97)00870-8.

[12] D.-M. Gomez-Coral *et al.*, *Deuteron and antideuteron production simulation in cosmic-ray interactions*, Phys. Rev. D **98**(2) (2018), doi:10.1103/PhysRevD.98.023012.

[13] M. Kachelriess *et al.*, *New calculation of antiproton production by cosmic ray protons and nuclei*, ApJ **803**(2), 54 (2015), doi:10.1088/0004-637X/803/2/54.

[14] A. Shukla *et al.*, *Large-scale simulations of antihelium production in cosmic-ray interactions*, Phys. Rev. D **102**(6) (2020), doi:10.1103/PhysRevD.102.063004.

[15] A. Ibarra and S. Wild, *Determination of the cosmic antideuteron flux in a Monte Carlo approach*, Phys. Rev. D **88**(2) (2013), doi:10.1103/PhysRevD.88.023014.

[16] D. Gomez Coral and A. Menchaca-Rocha, *SM antideuteron background to indirect dark matter signals in galactic cosmic rays*, J. Phys.: C. S. **1602**(1), 012005 (2020), doi:10.1088/1742-6596/1602/1/012005.

[17] L. J. Gleeson and W. I. Axford, *Solar modulation of galactic cosmic rays*, ApJ **154**, 1011 (1968), doi:10.1086/149822.

[18] M. Aguilar *et al.*, *The Alpha Magnetic Spectrometer (AMS) on the international space station: Part II — Results from the first seven years*, Phys. Rep. **894**, 1 (2021), doi:10.1016/j.physrep.2020.09.003.

[19] T. Aramaki *et al.*, *Review of the theoretical and experimental status of dark matter identification with cosmic-ray antideuterons*, Physics Reports **618**, 1 (2016), doi:10.1016/j.physrep.2016.01.002.

[20] Z. Weng, *AMS Measurements of Antiprotons and Antideuterons*, 38th International Cosmic Ray Conference (ICRC) (2023).

[21] K. Blum *et al.*, *Cosmic rays, antihelium, and an old navy spotlight*, Phys. Rev. D **96**(10) (2017), doi:10.1103/PhysRevD.96.103021.

[22] M. Korsmeier *et al.*, *Prospects to verify a possible dark matter hint in cosmic antiprotons with antideuterons and antihelium*, Phys. Rev. D **97**(10) (2018), doi:10.1103/PhysRevD.97.103011.

[23] P. D. L. T. Luque *et al.*, *Cosmic-ray propagation models elucidate the prospects for antinuclei detection*, J. Cosmol. Astropart. Phys. **2024**(10), 017 (2024), doi:10.1088/1475-7516/2024/10/017.